Modification of Primary Si Crystals and Fe-Rich Intermetallics in LM28 Al Alloy Fabricated Through Thixoforming

B. Sharif [1], H. Saghafian[1,2*] and S. H. Razavi [1]

* *saghafian@iust.ac.ir*

Received: September 2017 Accepted: January 2018

[1] School of Metallurgy and Materials Engineering, Iran University of Science and Technology Tehran, Iran.
[2] Center of Excellence for High Strength Alloys Technology (CEHSAT), Iran University of Science and Technology Tehran, Iran.
DOI: 10.22068/ijmse.15.2.32

Abstract: *In the present research, thixoforming route was carried out in order to enhance the microstructural features of LM28 piston alloy. Typical microstructure of this alloy was composed of coarse, polygonal primary silicon particles, eutectic matrix and intermetallic phases. Thermal analysis was carried out to study the solidification path of the base alloy and determine the major arrest temperatures of metallurgical reactions. Continuous and iso-thermal mechanical stirring were utilized to produce non-dendritic LM28 alloy feedstock for further processing. The rheocast samples were subjected to a rotation speed of 450 rpm. The slugs machined from the solidified rheocast specimens were heated in the mushy zone temperature and then were thixoformed via a laboratory press. The thixoformed specimens show a relatively homogenous microstructure and present no evidence of porosities. Fine, blocky primary silicon and Fe-rich intermetallic particles were uniformly distributed in the matrix of LM28 alloy. Optical microscope and scanning electron microscope linked with EDX were used to investigate the microstructure of specimens.*

Keywords: *Piston Alloy, Thermal Analysis, Thixoforming, Primary Silicon, Fe-Rich Intermetallic.*

1. INTRODUCTION

Piston Al-Si alloys such as LM28 are attracted by automotive industries for their unique combination of features including superior castability, reduced density combined with high mechanical properties at medium or elevated temperatures (nearly up to 623K (350°C)). Piston alloys are described by a eutectic matrix incorporating hard, angular primary silicon crystals together with complex intermetallic phases [1-10]. Improved mechanical strength and wear resistance of piston alloys are mainly attributed to the presence of fine, well dispersed primary silicon particles (PSPs) and eutectic silicon rods [4, 7, 11]. The addition of nickel and iron in hyper-eutectic Al-Si alloys enhances elevated temperature properties by precipitating thermally stable intermetallic particles which interrupt the movement of dislocations [8, 12, 13]. The size, morphology and distribution of primary silicon crystals, eutectic silicon and intermetallic phases have a vital influence on mechanical properties, tribological characteristics and machinability of the alloy [7, 8, 12-16].

The thermal analysis method is a recognized approach for studying the solidification path of Al-Si cast alloys. Significant metallurgical reactions are demonstrated on the cooling curve through curvature points and slope alterations [8, 17]. The first derivative of the cooling curve is derived in order to enhance the gradient variations in cooling curve which are associated to the solidification reactions of different phases. It also facilitates the estimation of nucleation time and temperature, solid fraction evolution and cooling rate of the primary and eutectic Si crystals in addition to different intermetallic phases precipitated during the solidification [9, 15].

Rheoprocessing involves intensive agitation of a liquid alloy (via pouring, stirring or vibration) either throughout solidification or isothermally at a specific fraction of solid for a determined duration of time [11, 18, 19]. The integrity of the agitation is characterized by a few factors, such as the shape of the stirrer, it's swirling speed and it's position relative to the melt surface and the crucible wall [20]. A number of technical considerations must be noted, which are also crucial in further processing of the semi-solid feedstock (e.g. Thixoforming). These include the solidification range, temperature process window, temperature sensitivity of the solid fraction,

morphological evolution and rheological properties [21].

In the case of hyper-eutectic Al-Si alloys, the semi-globular feed stock is reheated to the semi-solid state for subsequent production routes. In this condition the rheology will depend on the morphology and volume fraction of the existing solid phases which are composed of α-Al globules, primary silicon crystals and some intermetallic phases not remelted during reheating [1, 11, 21].

Thixoforming route has become a viable industrial process for manufacturing metallic materials specifically Al-Si cast alloys. Specimens which are acquired from the rheocasting section are reheated to the mushy zone temperature to stimulate the morphological alterations of solid phases. At this stage, in the semi-solid region, isothermal holding which causes partial remelting promotes the separation of α-Al globules and eutectic silicon phases. Furthermore it proliferates the quantity of semi-globular α-Al phase, generating a suitable microstructure for semi-solid forming [2, 3, 22]. Via thixoforming, the forming temperature, heat content and shrinkage of the semi-solid specimen can be significantly decreased. It will result in a fine, well dispersed primary silicon and intermetallic phases in a sound, free from porosity final product [1, 5, 6, 16, 22-24]. A major obstacle regarding the thixoforming process is the prevention of the liquid segregation phenomenon during deformation. In this phenomenon the liquid alloy with the composition of Al-Si eutectic is squeezed out to the free surface of the component. The main consequence of this segregation is an undesirable variation in mechanical properties of the thixoformed component [25, 26].

The present research was carried out to understand the effects of rheocasting (stirring) and thixoforming processes on the microstructural characteristics of LM28 piston alloy. Studying the solidification path of LM28 alloy will be done with the aid of cooling, first derivative and solid fraction curves. Stirring in the semi-solid region is done according to the liquidus and solidus temperatures obtained from cooling and first derivative curves. Furthermore, there have been few reports about intermetallic phases and their evolution after thixoforming, which were studied either.

2. EXPERIMENTAL PROCEDURE

Chemical composition of the LM28 alloy used in the present research is illustrated in table 1.

Table 1. Chemical composition of the aluminum alloy used in this study (wt.%).

Si	*Cu*	*Fe*	*Ni*	*Mg*	*Other impurity*	*Al*
18.20	*1.11*	*0.53*	*0.94*	*1.03*	*< 0.11*	*Bal.*

2. 1. Conventional Casting of LM28

In order to investigate the microstructural features of the base alloy, prior to further manufacturing procedures (mechanical stirring and thixoforming), a conventional casting route was performed. An estimated 600 grams of LM28 ingot was heated in a silicon carbide crucible to 993K (720°C) (nearly 80K super heat) in an electric resistance furnace. The melted alloy was then held isothermally at this temperature for a period of 30 minutes in order to homogenize the temperature of the liquid alloy in the crucible. Afterward, the oxide layer was skimmed from the surface of the melt. The molten LM28 alloy was then poured into graphite coated cylindrical steel molds, preheated to 323K (50°C). Thus, cylindrical specimens of 33 mm diameter, 100 mm height and a mass of 250 grams were obtained.

2. 2. Thermal Analysis

About 600 grams of LM28 alloy ingot was heated to 1053K (780°C) in the same SiC crucible and electric resistance furnace. Afterward, the molten alloy held isothermally at the mentioned temperature for a period of 30 minutes. Cooling curve thermal analysis (CCTA) was conducted by utilizing a graphite cup of 30 mm inner diameter, 70 mm height and 5 mm wall thickness. The cup was preheated to the molten alloy temperature by plunging in the melt for 15 minutes. Instantly, after sampling the molten LM28, a high sensitive K-type thermocouple was inserted into the melt, in the center of the cup, at a position of 10 mm from the bottom. In order to

avoid any vibration, thermocouple and graphite cup were assembled on a test stand. Thermal data was recorded by a high precision data acquisition system (A/D convertor) connected to a notebook computer. Simultaneously the continuous cooling curve and its first derivative curve were established with assistance of thermal analysis and excel software programs. The solid fraction evolution curve was acquired by calculating the integrated surface area between the first derivative of the cooling curve and the base line. The base line is representing the hypothetical first derivative of the cooling curve that does not exhibit metallurgical reactions during the solidification.

2. 3. P-Cu Master Alloy Modification

About 1200 grams of LM28 ingot was heated to 993K (720°C) and held isothermally at this temperature for 30 minutes. An estimated amount of 0.5 gram of Cu-20%P master alloy (equal to 0.0015 wt% P), wrapped in aluminum foil, was preheated before plunging into the liquid LM28 alloy. Afterward the liquid alloy was stirred by the same plunger for 1 minute in order to homogenize the alloy melt. Finally the modified liquid alloy was poured into cylindrical molds which were preheated to 323K (50°C).

2. 4. Mechanical Stirring

In the present study, in order to produce a semi-solid slurry of the LM28 alloy ingots, mechanical stirring was carried out. The same procedure conducted for the conventional casting of 600 grams of the base alloy was performed. After the homogenizing process of the molten alloy, the temperature of the melt was continuously reduced in the furnace to a predetermined temperature (863K (590°C)). So, the isothermal stirring of the alloy was performed at a temperature of about 50K (50°C) below the liquidus temperature and 25K (25°C) above the dendrite coherency point (DCP). A radial flow agitator fabricated with low carbon steel (CK45), coated with graphite and also preheated to 373K (100°C) was introduced into the semi-solid alloy. Swirling of the slurry was then started for a fixed duration of 10 minutes.

A continuous mechanical stirring of the partially solidified alloy was also investigated in this research. The temperature of the liquid alloy was reduced to 933K (660°C) (about 20K (20°C) above liquidus temperature). Subsequently, mechanical stirring was started while the temperature of the semi-solid slurry was continuously reduced. After 20 minutes of stirring, the temperature reduction of the slurry was about 90K (90°C). Finally the semi-solid alloy was poured into cylindrical molds at 843K (570°C) (about 5K (5°C) above DCP). In the case of continuous stirring, the cooling rate of the semi-solid slurry was 75×10^{-3} K (°C)/s.

In order to reduce the formation of vortex and avoiding the turbulence of the melt surface, position of the impeller blade, bottom of the SiC crucible and surface of the semi-solid alloy relative to each other was deeply considered. The convection intensity of the semi-solid slurry was controlled by adjusting the stirring speed of the agitator. In the present investigation 450 rpm (rotation per minute) was the main rotational speed of the stirrer. After each rheocasting test, the semi-solid slurry was poured into the same cylindrical steel molds which were coated with graphite and preheated to 323K (50°C). Fig. 1 shows the schematic illustration of the apparatus employed for rheocasting process.

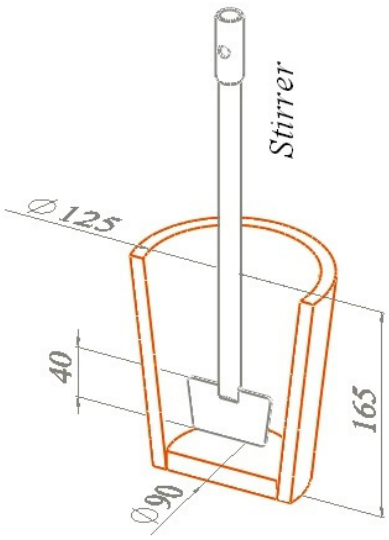

Fig. 1. Schematic illustration of the Stirring apparatus: stirrer and SiC crucible (Unit: mm).

2. 5. Thixoforming

For the thixoforming process, the rheocast and P-modified slugs were sectioned into 33 mm diameter and 50 mm height specimens. Afterward, the prepared slug was placed in the forming die which was fabricated and machined from carbon steel alloy and was coated with graphite. Thixoforming die was also lubricated with high temperature grease. A summary of the thixoforming processes which were conducted in this research is shown in table 2. Following that, the assembled thixoforming die (containing the sectioned feedstock) was located in a heat resistance furnace and then reheated to a predetermined temperature (851K (578°C) or 856K (583 °C)). The heating rate to mushy zone temperature, before thixoforming, was 0.1 K (°C)/s. The slug was then held isothermally at this temperature for a specific period of time (45 or 60 minutes). The temperature of the furnace was maintained constant within ± 1 K (°C) of the desired amount, which was corresponded to a particular fraction of solid. Thixoforming was performed via a laboratory press. A hydraulic cylinder was used to exert a uniaxial forming load of approximately 4 tones and then kept at this pressure for 30 seconds.

The ultimate speed of the ram (forming displacement) was adjusted on 4.6 mm/s, in order to exert a uniform and constant load on the semi-solid slug. Schematic figures of the casting and thixoforming specimens (sectioned horizontally) is presented in Fig. 2. According to this figure, the thixoforming specimen experienced a 45% reduction in height. The rheocast specimens were homogeneously compressed in the semi-solid region. The squeezed liquid alloy can be observed over the entire periphery of the solidified thixoformed specimen (Fig. 2-c). It is an illustration of a homogeneously thixoformed semi-solid alloy [27].

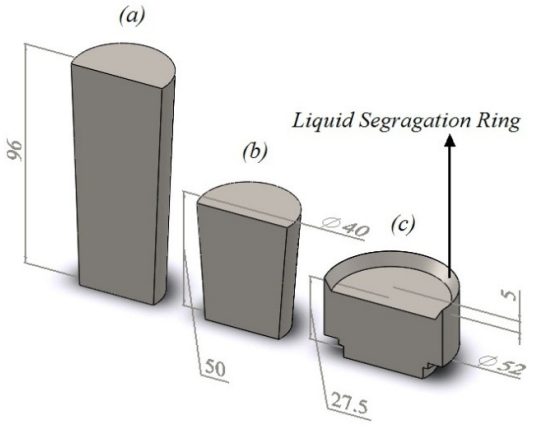

Fig. 2. Schematic figures of manufactured specimens (a) casting (b) feedstock before thixoforming (c) thixoformed specimen (Unit: mm).

2. 6. Material Analysis

The As-cast, rheocast and thixoformed samples were sectioned transversely and prepared with standard metallographic procedure. Microstructural characterization was primarily accomplished via an optical microscope equipped with an image acquisition system. The microstructure of the specimens were also analyzed by using a scanning electron microscope (Tescan-Vega II) coupled with an energy dispersive spectrometer (EDS) for elemental analysis.

Table 2. A summary of the Thixoforming processes.

Specimen code	*Mechanical Stirring Parameters*			*Thixoforming Parameters*	
	Stirring Speed (rpm)	*Temperature K(°C)*	*Time (min)*	*Holding Time (min)*	*Temperature K(°C)*
Thixo 1	*	*	*	*60*	*856 (583)*
Thixo 2	*450*	*863 (590)*	*10*	*60*	*856 (583)*
Thixo 3	*450*	*933-843 (660-570)*	*20*	*60*	*851 (578)*
Thixo 4	*450*	*863 (590)*	*10*	*45*	*856 (583)*

2. 7. Data Analysis

The circular diameter (average particle size) (d) for each primary silicon and intermetallic phase is calculated by assuming that the two dimensional (2-D) shape of the particles is circular. The circular diameter of each particle is given by:

$$d = 2 * \sqrt{\frac{A}{\pi}} \quad (1)$$

where A is the area of each solid particle on the sectioned surface.

The sphericity (S) of a particle is described as:

$$S = \frac{4 \pi A}{P^2} \quad (2)$$

where P is the perimeter of the particle. For S=1 the particle is a perfect circle while for lower shape factors (S<1) the particle has a complex morphology. Over 50 primary silicon and intermetallic particles were analyzed for each manufactured specimen and the average values of circular diameter and sphericity with their corresponding standard deviations were calculated.

3. RESULTS AND DISCUSSION

3. 1. As-Cast and P-Modified Specimens

The optical micrographs of the As-Cast and P-modified LM28 alloy are depicted in Fig. 3. The microstructure of the As-Cast and modified specimens are characterized by a dispersion of polygonal primary silicon crystals in a eutectic network of Al-Si phases together with various intermetallic compounds. These intermetallics are rich in nickel, copper and iron due to existence of these elements in the composition of LM28 alloy.

According to fig. 3a, high cooling rate is responsible for the small size of the PSPs (average circular diameter = 29.9 µm) which are approximately surrounded by α-Al phase. During solidification, silicon reduction in the vicinity of primary silicon crystals (and eutectic silicon matrix) in the liquid alloy, leads to a shift in chemical composition of the crystal's proximity and encourages the nucleation of α-Al phase [2, 5, 8]. Furthermore, the major characteristic of silicon eutectic phase is the rode-like morphology which indicates a high cooling rate during solidification [4, 16].

For the chemical modification of coarse PSPs, phosphorous is generally applied, due to the formation of AlP particles in the melt, on which silicon crystals can effectively nucleate. It can be attributed to the fact that both the crystal structure and lattice parameter of AlP compound is similar to that of primary silicon crystal. Phosphorus can be introduced into the liquid alloy in various methods such as red phosphorus, phosphate salt and Cu-P master alloy. In order to initiate the modification process, Cu3P phase needs to evolve to AlP compound. Poor modification of silicon particles is inevitable if the melting temperature is too low. Also because of the higher density of Cu-P master alloy

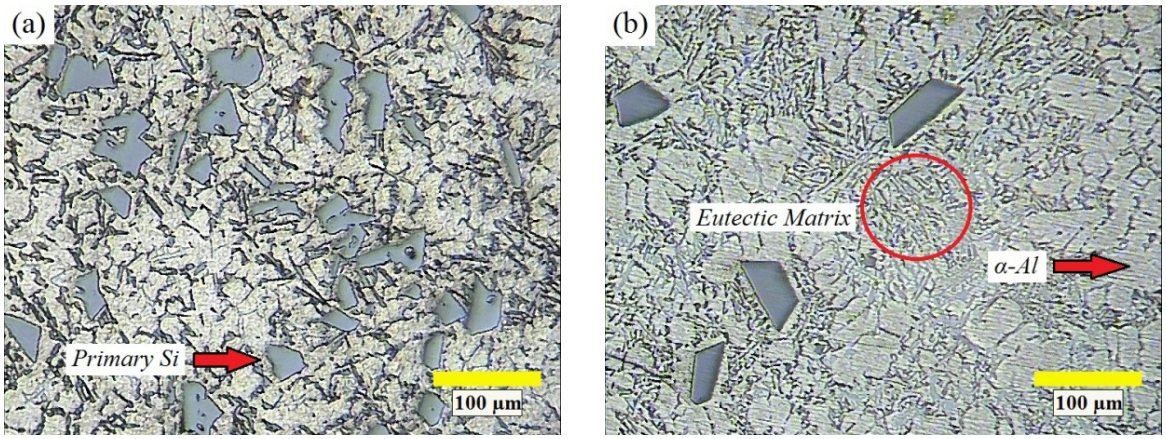

Fig. 3. Microstructure of LM28 alloy (a) As-Cast and (b) P-modified condition.

the Cu-P compounds may sediment and fall down to the bottom of the SiC crucible. These mentioned obstacles will inhibit the effective process of modification [28-32]. In the modified LM28 alloy (fig. 3b), the primary silicon crystals are relatively larger in size (average circular diameter = 50 μm) and their distribution in the matrix is less uniform. But, the PSPs have become modified and transformed to polygonal and blocky particles which are an exhibition of an effective phosphorus modification. In contrast with coarse, flake structure of eutectic silicon in the As-Cast specimen (Fig. 3a), eutectic silicon of P-modified sample is much finer and reduced in size. Some authors reported that the AlP particles have a key role in the nucleation of eutectic Si. The nucleation frequency of eutectic Si rods in P-contaminated liquid Al-Si alloys is often orders of magnitude higher compared to P-lean alloys [33].

3. 2. Thermal Analysis of LM28 Alloy

A combination of cooling and first derivative curves vs. Time for the LM28 alloy is depicted in Fig. 4. The cooling curve illustrates three main pulsations that indicate distinct transformations during the alloy solidification. These three major reactions, which are clearly illustrated via first derivative curve, are consisted of nucleation and growth of (a) primary silicon crystals (liquidus region), (b) Al-Si eutectic and (c) various intermetallic phases (especially Cu-enriched phases).

The primary silicon nucleation and growth interval (TP-Si) correlates with the first peak on the first derivative curve. This is the temperature corresponding to the commencing of the solidification process of the alloy. While maximum amount of each peak in the first derivative curve correlates with the growth temperature of a specific phase, it also coincides with the arrest temperature in the cooling curve. Arrest temperature is a turning point in the cooling curve where $d^2T/dt^2 = 0$ [17]. Nucleation and growth temperatures of primary silicon crystals are 650 °C and 640 °C respectively. The conventional average cooling rate which is calculated between the non-equilibrium liquidus (about 650 °C) and solidus temperatures (about 500 °C) is 0.28 °C/s. Also, the calculated solidification time for the thermal analysis specimen is about 800 seconds (13 minutes).

The amount of heat released (exothermic reaction) during the nucleation of a phase is proportional to the amount of precipitating phase, latent heat and enthalpy of transformation. Therefore, the integrated area between the first derivative curve and the base line (zero curve) is proportional to the solid fraction [9, 34]. According to solid fraction evolution vs. Temperature curve which is illustrated in Fig. 5, solidification range of the base alloy is about 150 °C. The temperature of 566 °C is the last point for the coarsening of the primary silicon crystals and the beginning of the Al-Si eutectic nucleation ($T_{Eu\text{-}Si}$). This is the temperature close to the dendrite coherency point (DCP) where

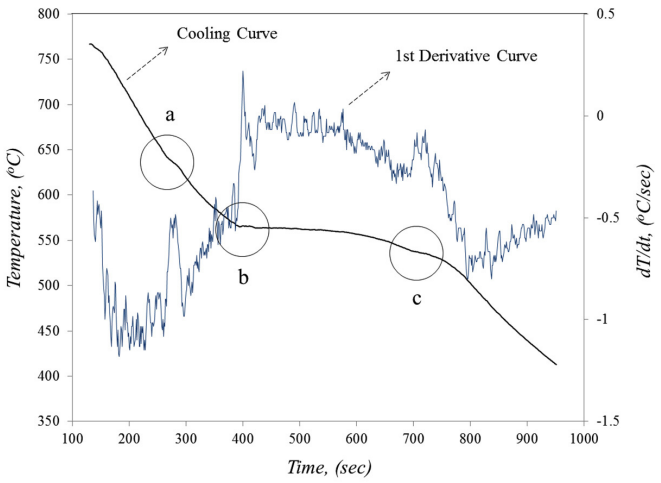

Fig. 4. Cooling and first derivative curves vs. Time for the LM28 alloy at cooling rate of 0.28 °C/s.

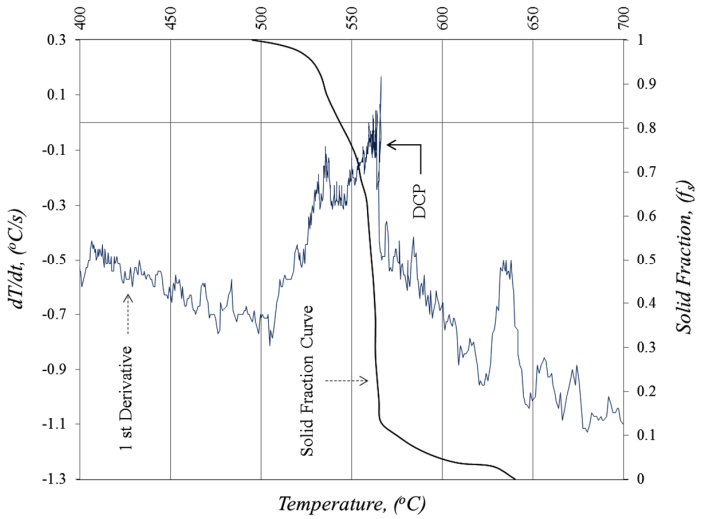

Fig. 5. Solid fraction and first derivative curves vs. Temperature for the LM28 alloy at cooling rate of 0.28 °C/s.

no apparent enlargement of the dendrites is going to happen, but they continue coarsening by the inter-dendritic feeding [8, 9]. Therefore in the vicinity of the Al-Si eutectic reaction and dendrite coherency point, a sudden increase in solid fraction is noted (Fig. 5). The Al-Cu enriched phases are solidified at temperature interval of 540°C and 530°C or below, which is also the final point of the dendritic coarsening.

3. 3. Mechanical Stirring Specimens

The rheocasting of partially solidified LM28 alloy, whether isothermally at a specific temperature or continuously in a wide range of solid fraction (or temperature), is characterized by a high shear rate and an efficient convection. Therefore a significant microstructural change is expected either in eutectic region and primary silicon crystals.

Fig. 6a depicts the P-modified microstructure of LM28 alloy. α-Al dendrites are surrounded by eutectic silicon and coarse PSPs. In the case of mechanical stirring, dendrite arm fragmentation is the dominant mechanism responsible for microstructural evolution of LM28 alloy. α-Al dendrite arms bend under the applied shear force and inevitably detach if the critical shear stress is reached. This phenomenon is clearly illustrated in Fig. 6b, where a few of the α-Al dendrite arms are separated from the main α-Al dendrite. In contrast to P-modified condition (Fig. 6a), α-Al dendrites

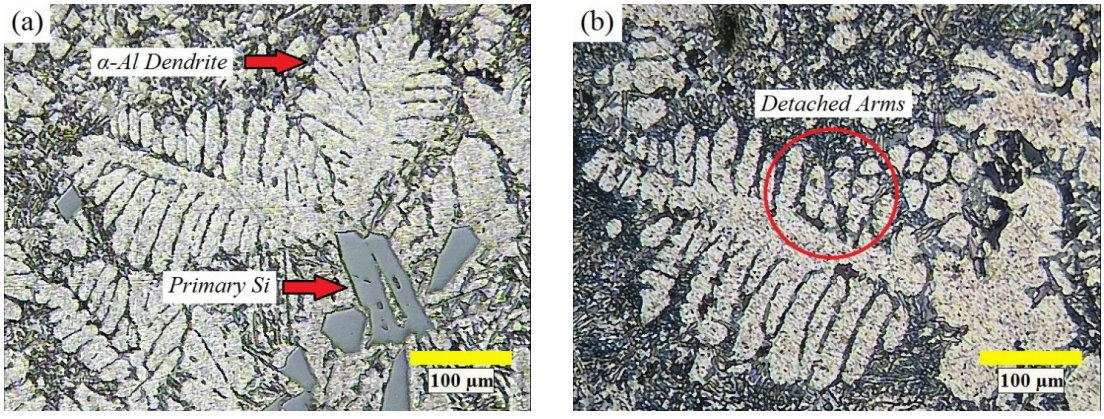

Fig. 6. Microstructure of LM28 eutectic matrix for (a) P-modified and (b) Stirred (450 r/min-590 °C) specimens.

are relatively coarser and eutectic silicon are much finer in stirred condition [11, 19, 35].

Mechanical stirring either isothermally or continuously in the semi-solid region promotes the separation of α-Al solid solution and eutectic silicon phases and subsequently increases the volume fraction of the non-dendritic α-Al phase. During stirring, the Al atoms in the solution can easily precipitate on the existing α-Al phase, and then these globules will spheroidize and coarsen under the driving force of decreasing the interfacial free energy. It results in a microstructure with superior rheological properties [2, 3, 11, 35]. The volume fraction of α-Al phase increases from 0.68 for the As-Cast specimen to 0.76 for the stirred sample (450 r/min-590 °C) (over 10 percent increase). As the stirring time increases, more particles are generated and then they are more prone to become clustered and attached to each other [11, 18]. As shown in Fig. 7a, the agglomerated α-Al globules are segregated from fine eutectic silicon particles. According to Fig. 7b some intermetallic phases (mainly Mg2Si) are precipitated between α-Al globules.

Also, an increase of the size of primary silicon crystals was observed (Fig. 8b). This indicates that the stirring in semi-solid region promotes the coarsening of silicon particles. This phenomenon is also reported in other manuscripts [10, 11].

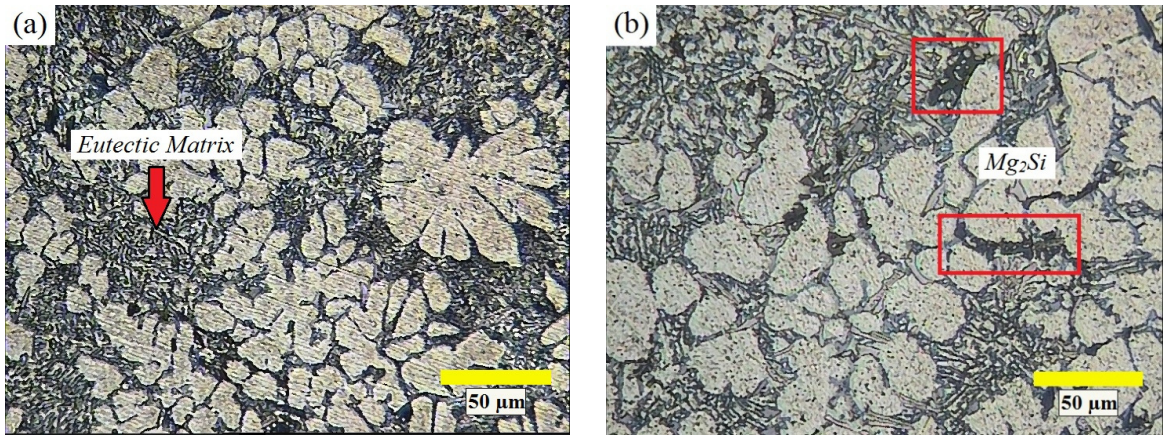

Fig. 7. Microstructure of eutectic matrix of (a) Stirred (450 r/min - 660 °C-570 °C) and (b) Stirred (450 r/min-590 °C) specimens.

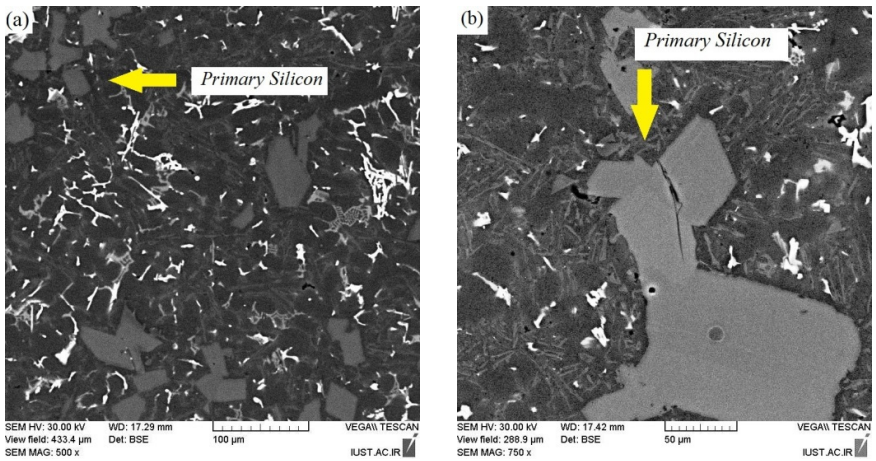

Fig. 8. SEM images of (a) P-modified LM28 (500x) (b) Stirred (450 r/min-590 °C) (750x).

3. 4. Thixoforming Specimens

In the process of thixoforming, the upper punch moved down and pressed the reheated specimen to the final shape. Afterward, the forming pressure was being exerted on the specimen for a period of 30 seconds. This allows the thixoformed component to solidify under a 4 tones uniaxial pressure. Therefore, all of the manufactured specimens were free from micro and macro porosities which had been observed in the rheocasting specimens due to shrinkage [22, 25, 36, 37]. Some liquid penetration of eutectic composition was observed mainly in the upper portion of the thixoformed parts. Most of the liquid phase would considerably accumulate heavily at the regions where is far away from the loading center [22, 24]. For the thixoformed components, the amount of liquid segregation is less than 5 pct which is acceptable in this process.

α-Al rosettes and globules, which had formed during rheocasting process, were experienced a remarkable spheroidization and ripening during reheating to thixoforming temperature. Also, during the reheating and then, holding the specimen in the mushy zone temperature, the Cu and Mg enriched intermetallic phases remelt while the remnants of the eutectic (mainly Fe-rich phases) remain solid but experience a significant microstructural transformation [1, 36, 38]. A fraction of dissolved Si and Al have deposited on the PSPs and α-Al globules respectively. The fine blocky PSPs are uniformly spread in the matrix of α-Al phase. The thixoformed specimens manifest a relatively homogenous microstructure and present no evidence of porosities and shrinkage holes [7]. Optical micrographs of thixoformed specimens are illustrated in Fig. 9.

Activation of the diffusion process at elevated temperatures encourages the microstructural alterations of α-Al and eutectic Si phase.

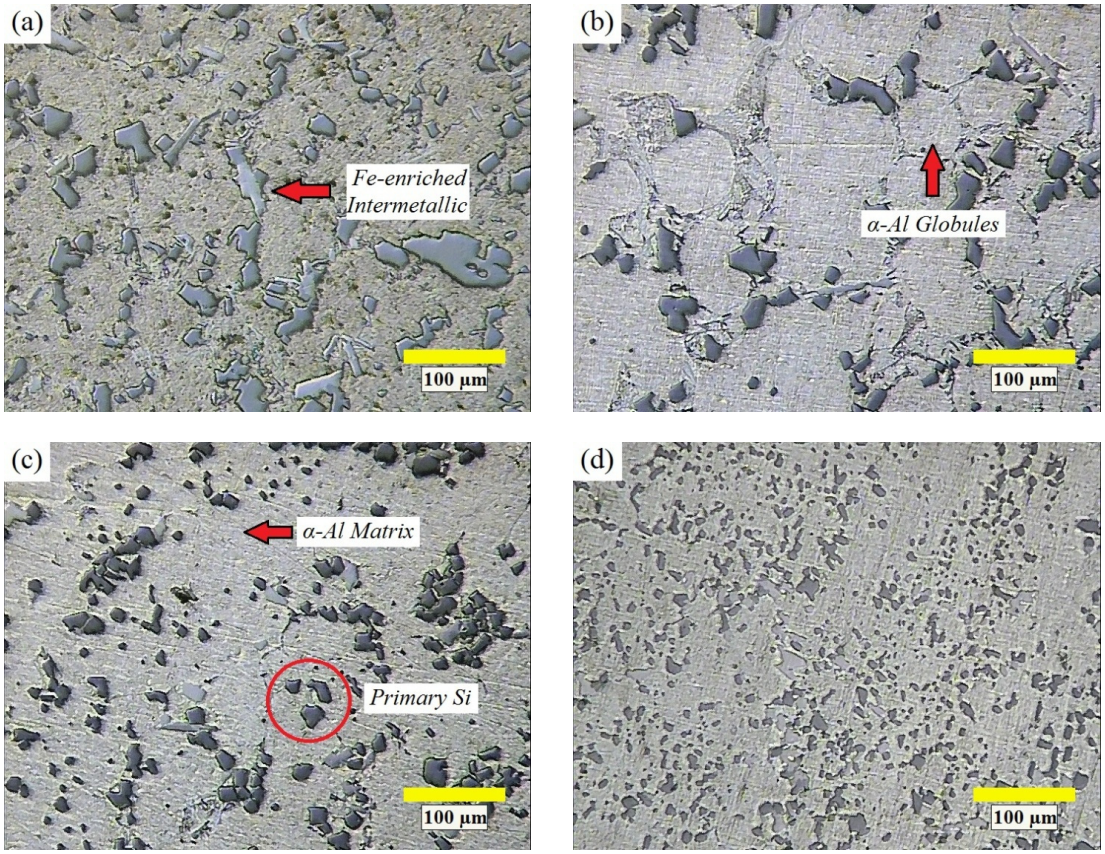

Fig. 9. Microstructure of Thixoforming specimens (a) Thixo 1 (b) Thixo 2 (c) Thixo 3 (d) Thixo 4.

Therefore, in order to minimize the risks of grain coarsening (in the reheating period) the holding time and temperature should be decreased while the heating rate of the specimen should be increased [19]. In the case of Thixo 3 specimen (Fig. 9c), the heating temperature is reduced to 578 °C (5 °C reduction). Therefore the liquid fraction for the thixoforming is reduced and as a result, the solid portion of the reheated alloy, deformed more severely during forming. In the case of Thixo 4 component (Fig. 9d), the holding time before thixoforming is reduced to 45 min (a 15 min reduction), resulting to an increase of the solid fraction of the semi-solid slug. Therefore, the semi-solid feedstock experiences a higher deformation rate [37]. Lowering the heating temperature and holding time resulted in a more refined microstructure. The average circular diameter of the primary silicon and intermetallic particles decreases remarkably for the Thixo 3 and Thixo 4 components and the roundness of the primary silicon and intermetallic phases also enhanced.

The circular diameter and sphericity of primary silicon crystals for As-cast and thixoformed specimens are shown in figs. 10 and 11 respectively. According to these figures, primary silicon refinement is successfully achieved by thixoforming process. In comparison, the extent of microstructural refinement is more remarkable for Thixo 4 when the holding time (before thixoforming) is reduced to 45 minutes. It was also observed that thixoforming minimized the variation of primary

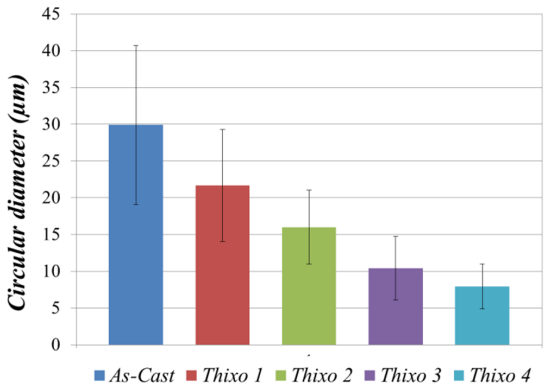

Fig. 10. Circular diameter (d) of PSPs for As-Cast and Thixo specimens.

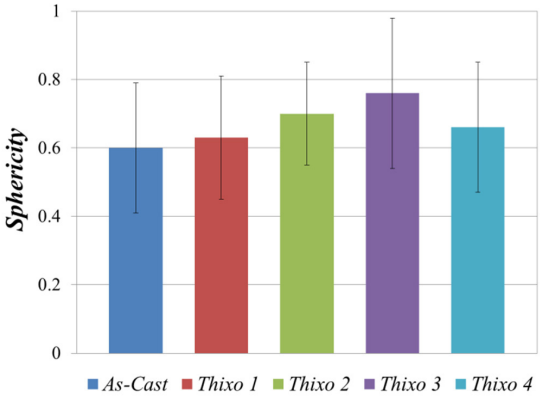

Fig. 11. Sphericity (S) of PSPs for As-Cast and Thixo specimens.

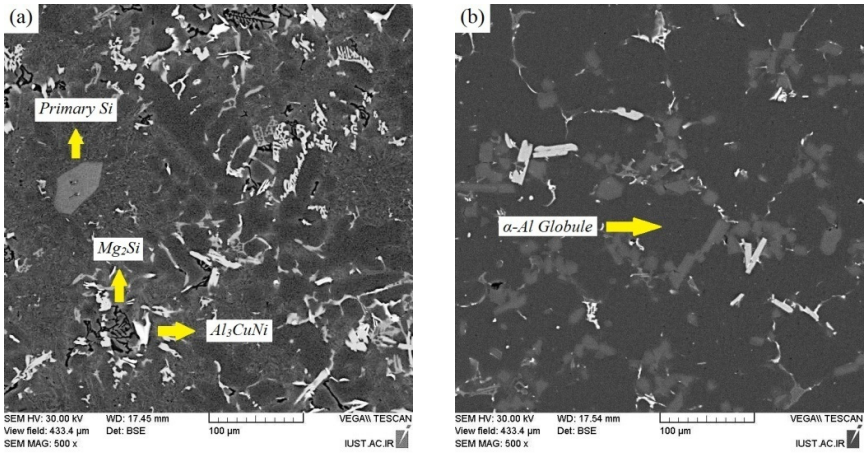

Fig. 12. SEM images of (a) Stirred (450 r/min-590 °C) and (b) Thixo 2.

silicon crystal size that is represented by the smaller standard deviations (Fig. 10).

During the reheating to the thixoforming temperature, the eutectic phase which is generally concentrated at grain boundaries begin to melt. The α-Al grains turn to be more globular due to the effect of interface curvature. Also PSPs remain solid through the reheating process. During the deformation process, a fraction of the eutectic melt squeezed from the loading center and consequently, low melting point alloying elements were transferred to the free surface of the thixoformed component. Therefore, the amounts of the alloying elements are fewer in the lower parts of the thixoformed specimen. In contrast, high melting point alloying elements such as Fe and Ni remained in the microstructure, in the form of compact, polygonal intermetallic phases with expected benefits regarding the ductility of the thixoformed parts [22, 24]. SEM images and X-ray mapping analysis of elemental distribution of Stirred (450 r/min-590 °C) and Thixo 2 specimens are illustrated in Figs. 12 and 13, respectively. According to Fig. 13, the

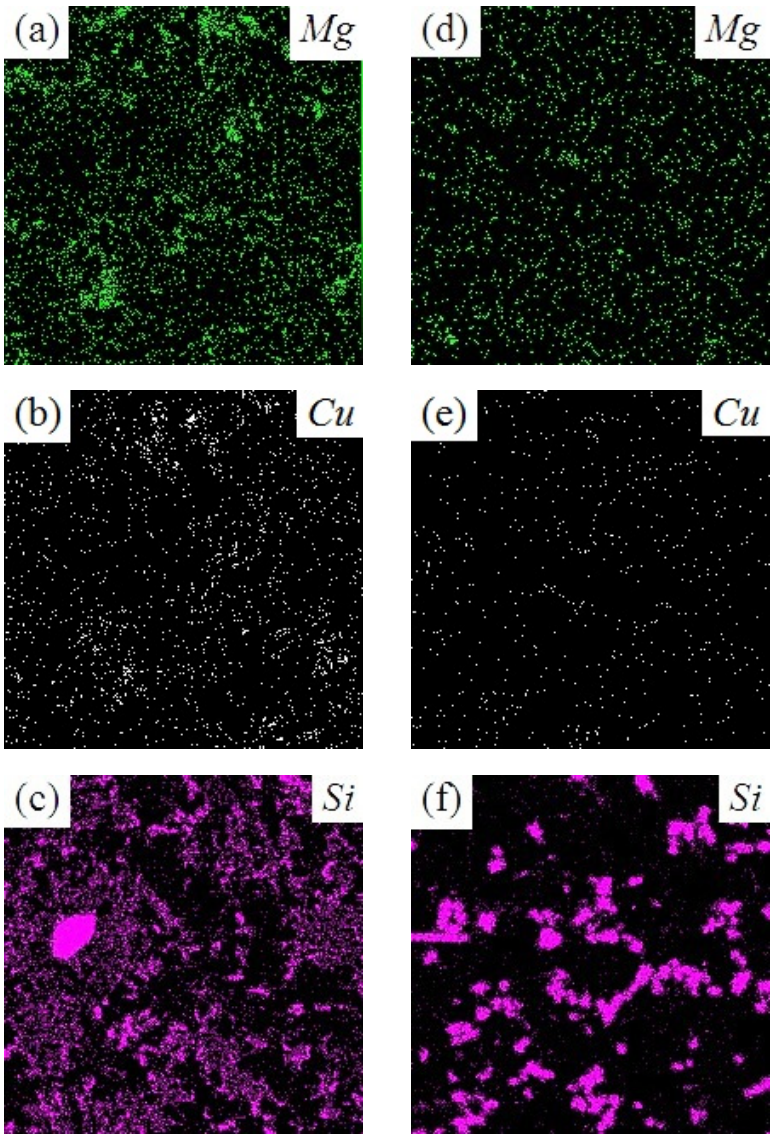

Fig. 13. X-ray maps of elemental distribution of Fig. 12a (left side a-c) and Fig. 12b (right side d-f).

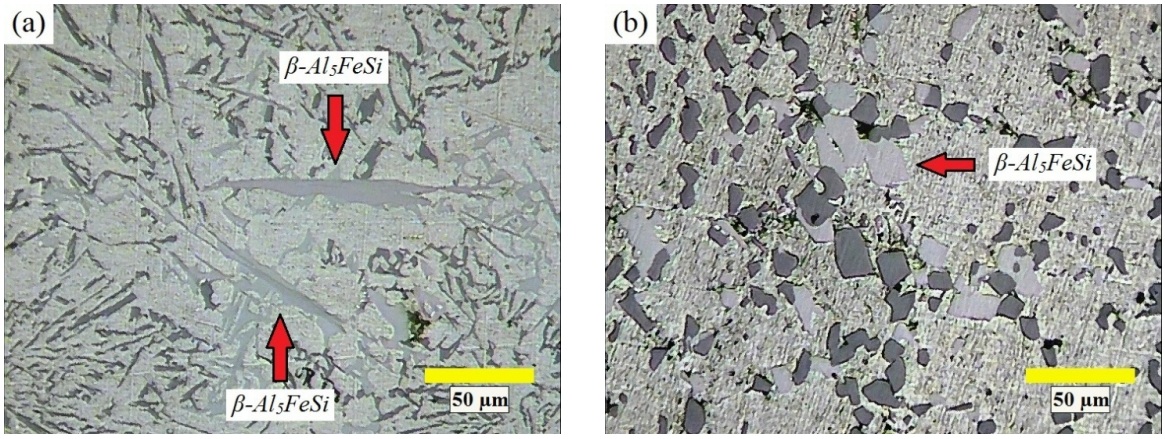

Fig. 14. Microstructures of (a) Stirred (450 r/min-590 °C) and (b) Thixo 4 specimens.

elemental concentration of alloying elements (Mg, Cu and Si) is relatively faded after thixoforming process. As mentioned above, during the forming process a small portion of the liquefied eutectic move between the PSPs and α-Al globules and accumulate in the free surface of the thixoformed alloy. Therefore, the chemical composition of the thixoformed parts deviate from the LM28 composition. Since the squeezed melt, which is solidified in the form of a conical ring, forms only 5% (volumetric) of the thixoformed slug, the deviation from the main chemical composition is negligible [39].

The presence of iron in the base alloy causes the precipitation of needle-like, Fe-rich intermetallics in the matrix as shown in Fig. 14a. β-Al5FeSi is the most frequent Fe-rich intermetallic phase and is responsible for the decrease of the mechanical properties. Angular PSP's and sharp-edged iron-rich intermetallics facilitate the nucleation of cracks owing to high stress concentration at the particle-matrix interface and provide easy path for fracture, consequently deteriorating the ductility and tensile strength of the alloy [30, 40, 41]. Material deformation during thixoforming causes the fragmentation of hard intermetallic phases and significantly reduces the negative effects of platelet intermetallics. This phenomenon is also applicable for the primary Si crystals. Fig. 14b illustrates the fine, polygonal primary Si and intermetallic particles distributed in the α-Al matrix.

Fig. 15a shows the BSE (back scattered

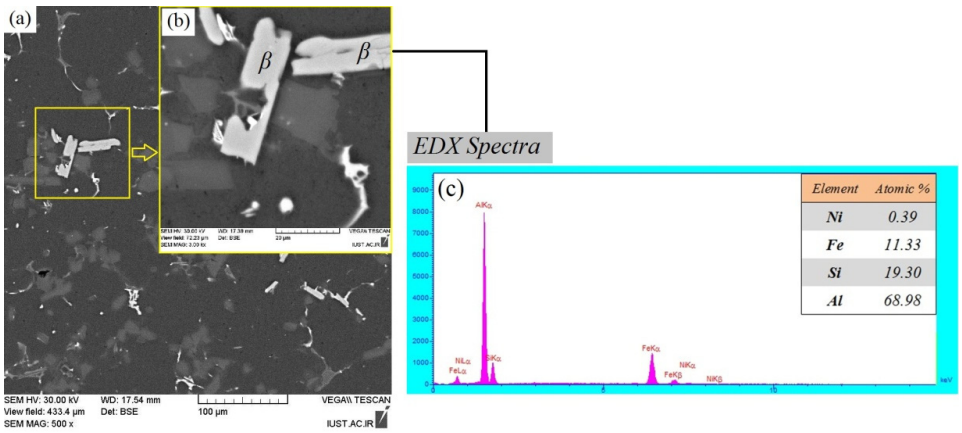

Fig. 15. (a) SEM micrograph of Thixo 2 specimen (b) magnified micrograph of β-Al5FeSi (c) EDX analysis result of β-Al5FeSi shown in the micrograph (b).

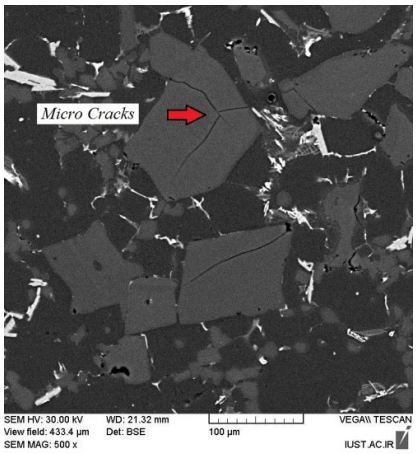

Fig. 16. Micro cracks on PSPs for Thixo 2 specimen.

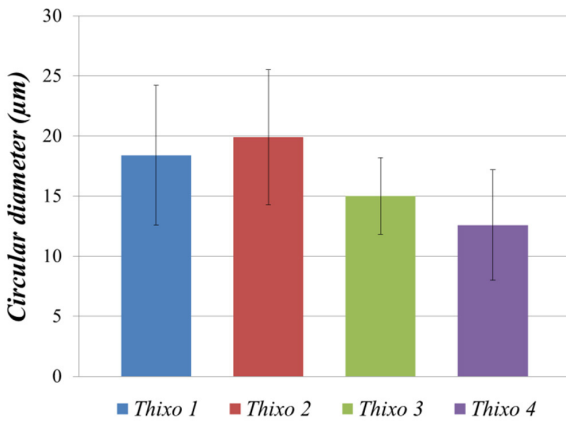

Fig. 17. Circular diameter (d) of Fe-rich intermetallic particles for Thixo specimens.

electron) image of Thixo 2 specimen showing compact, polygonal intermetallic particles which are also magnified in Fig.15b. Fig. 15c illustrates the corresponding EDX spectra for the marked intermetallic particles (β) in Fig. 15b. The atomic concentrations of the Al, Fe and Si were in a good agreement with the concentrations obtained for the β-Al5FeSi by others [11, 12].

Micro cracks are clearly observed on PSPs (Fig. 16). This is due to simultaneous plastic deformation and flow of α-Al globules in the vicinity of primary silicon and intermetallic phases. These phases have confined or no formability and also have a high stress concentration sensibility and as a result would cause cracking under thixoforming pressure. These micro cracks can propagate in the structure of brittle phases and finally break them into fine, blocky particles (PSPs & β-Al5FeSi) which is also observed in Fig. 14b [22, 25].

The circular diameter and sphericity of Fe-rich intermetallics for thixoformed specimens are also illustrated in Figs. 17 and 18 respectively. Fe-rich intermetallic phases which were supposed to have complex morphologies (needle-like shapes) experience a significant reduction in average particle size after thixoforming process. Furthermore, the modification of these hard, brittle phases enhances and consequently leads to superior mechanical properties.

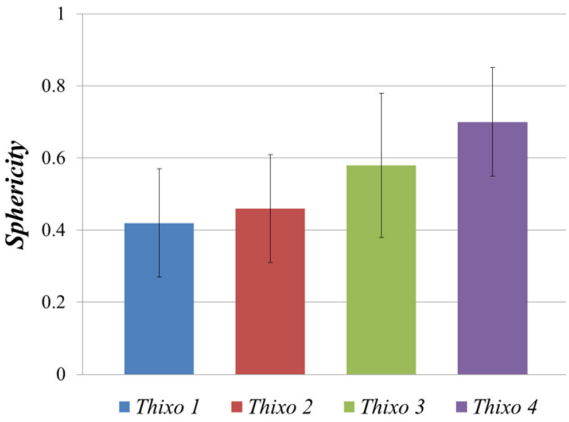

Fig. 18. Sphericity (S) of Fe-rich intermetallic particles for Thixo specimens.

CONCLUSIONS

The results are summarized as follow:

1. Mechanical stirring either isothermally or continuously in the semi-solid region promotes the separation of α-Al solid solution and eutectic silicon phases and subsequently increases the volume fraction of the non-dendritic α-Al phase. Mechanical stirring of hyper-eutectic Al-Si alloys in the semi-solid region promotes the coarsening of silicon particles.
2. Liquid penetration of eutectic composition is observed mainly in the upper portion of the thixoformed parts. During the

thixoforming process, a fraction of the eutectic melt squeezed from the loading center and consequently, low melting point alloying elements were moved to the free surface of the deformed component.

3. In order to minimize the risks of grain coarsening, the reheating temperature and holding time should be decreased. Refinement of primary silicon and intermetallic particles is successfully achieved by thixoforming process.
4. Material deformation during thixoforming causes the fragmentation of hard intermetallic phases and significantly reduces the negative effects of platelet intermetallics. This phenomenon is also applicable for the primary Si crystals.
5. Fe-rich intermetallic phases (mainly β-Al5FeSi) experience a significant reduction in average particle size after thixoforming process. The modification of these hard, brittle phases enhances and consequently leads to superior mechanical properties.

REFERENCES

1. Kapranos, P., Kirkwood, D. H., Atkinson, H. V., Rheinlander, J. T., Bentzen, J. J., Toft, P. T., "Thixoforming of an automotive part in A390 hypereutectic Al–Si alloy", J. Mater. Process. Technol., 2003, 135, 271-277.
2. Lashkari, O., Ajersch, F., Charette, A., Chen, X. G., "Microstructure and rheological behavior of hypereutectic semi-solid Al–Si alloy under low shear rates compression test", Mater. Sci. Eng., A, 2008, 492, 377-382.
3. Tebib, M., Morin, J. B., Ajersch, F., Grant Chen, X., "Semi-solid processing of hypereutectic A390 alloys using novel rheoforming process", Trans. Nonferrous Met. Soc. China, 2010, 20, 1743-1748.
4. Hekmat-Ardakan, A., Liu, X., Ajersch, F., Chen, X. G., "Wear behaviour of hypereutectic Al–Si–Cu–Mg casting alloys with variable Mg contents", Wear, 2010, 269, 684-692.
5. Birol, Y., "Cooling slope casting and thixoforming of hypereutectic A390 alloy", J. Mater. Process. Technol., 2008, 207, 200-203.
6. Birol, Y. B. a. F., "Wear properties of thixoformed AlSiCuFe alloys", INT J MATER FORM, 2008, 1, 981-984.
7. Lasa, L., Rodriguez-Ibabe, J. M., "Wear behaviour of eutectic and hypereutectic Al–Si–Cu–Mg casting alloys tested against a composite brake pad", Mater. Sci. Eng., A, 2003, 363, 193-202.
8. Manasijevic, S., Radisa, R., Markovic, S., Acimovic-Pavlovic, Z., Raic, K., "Thermal analysis and microscopic characterization of the piston alloy $AlSi1_3Cu_4Ni_2Mg$", Intermetallics, 2011, 19, 486-492.
9. Robles Hernández, F. C., Sokolowski, J. H., "Thermal analysis and microscopical characterization of Al–Si hypereutectic alloys", J. Alloys Compd., 2006, 419, 180-190.
10. Hekmat-Ardakan, A., Ajersch, F., "Effect of isothermal ageing on the semi-solid microstructure of rheoprocessed and partially remelted of A390 alloy with 10% Mg addition", Mater. Charact., 2010, 61, 778-785.
11. Hekmat-Ardakan, A., Ajersch, F., "Effect of conventional and rheocasting processes on microstructural characteristics of hypereutectic Al–Si–Cu–Mg alloy with variable Mg content", J. Mater. Process. Technol., 2010, 210, 767-775.
12. Abouei, V., Shabestari, S. G., Saghafian, H., "Dry sliding wear behaviour of hypereutectic Al–Si piston alloys containing iron-rich intermetallics", Mater. Charact., 2010, 61, 1089-1096.
13. Taghiabadi, R., Ghasemi, H. M., Shabestari, S. G., "Effect of iron-rich intermetallics on the sliding wear behavior of Al–Si alloys", Mater. Sci. Eng., A, 2008, 490, 162-170.
14. Kotadia, H. R., Hari Babu, N., Zhang, H., Fan, Z., "Microstructural refinement of Al–10.2%Si alloy by intensive shearing", Mater. Lett., 2010, 64, 671-673.
15. Shabestari, S. G., Malekan, M., "Assessment of the effect of grain refinement on the solidification characteristics of 319 aluminum alloy using thermal analysis", J. Alloys Compd., 2010, 492, 134-142.
16. Vencl, A., Bobić, I., Mišković, Z., "Effect of thixocasting and heat treatment on the tribological properties of hypoeutectic Al–Si alloy", Wear, 2008, 264, 616-623.
17. Shabestari, S. G., Ghoncheh, M. H., Momeni,

H., "Evaluation of formation of intermetallic compounds in Al2024 alloy using thermal analysis technique", Thermochim Acta, 2014, 589, 174-182.
18. Canyook, R., Wannasin, J., Wisuthmethangkul, S., Flemings, M. C., "Characterization of the microstructure evolution of a semi-solid metal slurry during the early stages", Acta Mater., 2012, 60, 3501-3510.
19. Sukumaran, K., Pai, B. C., Chakraborty, M., "The effect of isothermal mechanical stirring on an Al–Si alloy in the semisolid condition", Mater. Sci. Eng., A, 2004, 369, 275-283.
20. Hashim, J., Looney, L., Hashmi, M. S. J., "Metal matrix composites: production by the stir casting method", J. Mater. Process. Technol., 1999, 92–93, 1-7.
21. Nafisi, S., Ghomashchi, R., "Impact of melt treatment on semi-solid metal processing", J. Alloys Compd., 2007, 436, 86-90.
22. Chen, G., Du, Z., Cheng, Y., "Effect of mechanical conditions on the microstructures and mechanical properties of thixoformed Al–Cu–Si–Mg alloy", Mater. Des., 2012, 35, 774-781.
23. Jung, H. K., Kang, C. G., "Reheating process of cast and wrought aluminum alloys for thixoforging and their globularization mechanism", J. Mater. Process. Technol, 2000, 104, 244-253.
24. Birol, Y., "Forming of $AlSi_8Cu_3Fe$ alloy in the semi-solid state", J. Alloys Compd., 2009, 470, 183-187.
25. Kang, C. G., Youn, S. W., Seo, P. K., "Data base construction on mechanical properties of thixoforged aluminum parts and their microstructure evaluation", Journal J. Mater. Process. Technol, 2005, 159, 330-337.
26. Cavaliere, P., Cerri, E., Leo, P., "Effect of heat treatments on mechanical properties and damage evolution of thixoformed aluminium alloys", Mater. Charact., 2005, 55, 35-42.
27. Fukui, Y., Nara, D., Kumazawa, N., "Evaluation of the Deformation Behavior of a Semi-solid Hypereutectic Al-Si Alloy Compressed in a Drop-Forge Viscometer", Metall. Mater. Trans. A, 2015, 46, 1908-1916.
28. Gao, T., Zhu, X., Qiao, H., Liu, X., "A new Al–Fe–P master alloy designed for application in low pressure casting and its refinement performance on primary Si in A390 alloy at low temperature", J. Alloys Compd., 2014, 607, 11-15.
29. Cao, F., Jia, Y., Prashanth, K. G., Ma, P., Liu, J., Scudino, S., "Evolution of microstructure and mechanical properties of as-cast Al-50Si alloy due to heat treatment and P modifier content", Mater. Des., 2015, 74, 150-156.
30. Wu, F. F., Li, S. T., Zhang, G. A., Jiang, F., "Microstructural evolution and mechanical properties of hypereutectic Al-Si alloy processed by liquid die forging", Bull. Mater. Sci., 2014, 37, 1153-1157.
31. Dai, H., Liu, X., "Effects of individual and combined additions of phosphorus, boron and cerium on primary and eutectic silicon in an Al-30Si alloy", Rare Metals, 2009, 28, 651-655.
32. Wang, R., Lu, W., "Microstructural Characteristic and Mechanical Behavior of Nodular Silicon Hypereutectic Al-Si Alloys", JOM, 2012, 64, 330-336.
33. Ludwig, T. H., Schonhovd Dæhlen, E., Schaffer, P. L., Arnberg, L., "The effect of Ca and P interaction on the Al–Si eutectic in a hypoeutectic Al–Si alloy", J. Alloys Compd., 2014, 586, 180-190.
34. Yamagata, H., Kurita, H., Aniolek, M., Kasprzak, W., Sokolowski, J. H., "Thermal and metallographic characteristics of the Al–20% Si high-pressure die-casting alloy for monolithic cylinder blocks", J. Mater. Process. Technol, 2008, 199, 84-90.
35. Nafisi, S., Ghomashchi, R., "Effect of stirring on solidification pattern and alloy distribution during semi-solid-metal casting", Mater. Sci. Eng., A, 2006, 437, 388-395.
36. Shabestari, S. G., Parshizfard, E., "Effect of semi-solid forming on the microstructure and mechanical properties of the iron containing Al–Si alloys", J. Alloys Compd., 2011, 509, 7973-7978.
37. Kopp, R., Neudenberger, D., Winning, G., "Different concepts of thixoforging and experiments for rheological data", J. Mater. Process. Technol, 2001, 111, 48-52.
38. Benati, D., Zoqui, E., "Effect of Silicon on the Thixoformability of Al-Si-Cu Alloys", J. Mater. Eng. Perform., 2014, 23, 3165-3179.

39. Gencalp Irizalp, S., Saklakoglu, N., "Effect of Fe-rich intermetallics on the microstructure and mechanical properties of thixoformed A380 aluminum alloy", JESTECH, 2014, 17, 58-62.
40. Kaur, P., Dwivedi, D. K., Pathak, P. M., "Effects of electromagnetic stirring and rare earth compounds on the microstructure and mechanical properties of hypereutectic Al–Si alloys", IJAMT, 2012, 63, 415-420.
41. Guan, R. G., Zhao, Z. Y., Lee, C., Zhang, Q. S., Liu, C. M., "Effect of Wavelike Sloping Plate Rheocasting on Microstructures of Hypereutectic Al-18 pct Si-5 pct Fe Alloys", Metall. Mater. Trans. B, 2012, 43, 337-343.